PROCEEDINGS OF SPIE

SPIEDigitalLibrary.org/conference-proceedings-of-spie

Asymmetric cross-polarization coupling between microresonator whispering-gallery modes

Sandoval, Karleyda, Junaid Ul Haq, Mohmad, Rosenberger, A.

Karleyda Sandoval, Mohmad Junaid Ul Haq, A. T. Rosenberger, "Asymmetric cross-polarization coupling between microresonator whispering-gallery modes," Proc. SPIE 12016, Optical and Quantum Sensing and Precision Metrology II, 120160D (2 March 2022); doi: 10.1117/12.2617251

SPIE.

Event: SPIE OPTO, 2022, San Francisco, California, United States

Asymmetric cross-polarization coupling between microresonator whispering-gallery modes

Karleyda Sandoval, Mohmad Junaid Ul Haq, and A. T. Rosenberger*
Department of Physics, Oklahoma State University, Stillwater, OK, USA 74078-3072

ABSTRACT

Theoretical calculation of the cross-polarization coupling between whispering-gallery modes in a microresonator shows that this coupling is, in general, asymmetric. The spin-orbit induced coupling of light from a TE mode to a coresonant TM mode will have a different strength than that of the coupling from the TM mode to the TE mode. This coupling asymmetry is confirmed in coupled-mode induced transparency experiments. By monitoring the throughput spectrum in both polarizations when the input directly excites only modes of one polarization, the coupling strengths in both directions are determined simultaneously by fitting to a model. Some examples and implications are discussed here.

Keywords: microresonator, whispering-gallery modes, induced transparency, nonreciprocal cross-polarization coupling

1. INTRODUCTION

Microresonator systems can exhibit coupled-mode induced transparency (CMIT) and Autler-Townes splitting (ATS) with pulse delay, and coupled-mode induced attenuation (CMIA) with pulse advancement or delay, when there is coupling between two coresonant modes.[1-3] These behaviors may be exploited for numerous applications such as signal processing and optical sensing.[4-6] Polarization effects are of growing interest,[7-12] and induced transparency is even possible in a system without mode coupling when two orthogonally polarized coresonant modes are simultaneously excited by light polarized at 45° and the same polarization is detected, as presented elsewhere in this conference (12016-174).[13] The mode coupling under study in the present work is cross-polarization coupling, resulting from the spin-orbit interaction of light in a microresonator's whispering-gallery modes (WGMs).[14] The interaction between the spin and extrinsic orbital angular momentum of light in a WGM causes a weak polarization rotation, resulting in cross-polarization coupling (CPC). The different axial extent of the coupled modes, one TE (transverse electric) and one TM (transverse magnetic), then results in their coupling being nonreciprocal. Here we describe a method for experimentally determining the CPC strengths of TE to TM coupling and TM to TE coupling in a hollow bottle resonator (HBR).[15]

In previous work, the throughput spectrum of the input polarization has been studied to analyze the CMIT, ATS, and CMIA features and find the CPC strength by fitting to a model.[1] If the CPC amplitudes are t_{21} for coupling from mode 1 (input) to mode 2 and $-t_{12}$ for 2 to 1 coupling (see Fig. 1), the destructive interference that gives CMIT comes from light coupled from 1 to 2 and back into 1, so that this contribution to the intracavity mode 1 field amplitude picks up a factor of $-T_c = -t_{21}t_{12}$. Model fitting then determines T_c. In other previous work, the CPC strength T_c has also been determined by amplitude-modulating the input.[16,17] Finding the modulation frequency that gives the minimum amplitude of the modulated mode 1 throughput on resonance gives a value of T_c that agrees with the value determined by model fitting, at least in the case of CMIT or ATS. (If T_c is large enough, there is actual frequency splitting and the IT feature evolves into ATS.[1,17])

In the work presented here, in addition to fitting the mode 1 throughput, the mode 2 throughput is also fitted, determining the ratio $b = t_{21}/t_{12}$, since the mode 2 throughput amplitude is proportional to t_{21}. The fact that throughput on mode 2 is observed is evidence for the existence of CPC, and knowing b and T_c allows us to determine both t_{21} and t_{12}, demonstrating the nonreciprocity of CPC. Also, T_c and b are calculated, using the theory presented in Ref. 14, for a representative set of mode numbers that give values of T_c and b similar to those determined experimentally. These calculations give examples of what the transverse profiles of typical cross-polarization coupled modes might look like.

*atr@okstate.edu; phone 1 405 744-6742; fax 1 405 744-6811; rosenberger.okstate.edu

Optical and Quantum Sensing and Precision Metrology II, edited by
Jacob Scheuer, Selim M. Shahriar, Proc. of SPIE Vol. 12016, 120160D
© 2022 SPIE · 0277-786X · doi: 10.1117/12.2617251

2. MODEL AND THEORY

We use a ring cavity model as shown in Fig. 1. In In Fig. 1, the subscripts 1 and 2 refer to the two orthogonal polarizations. E_{fj} is the input amplitude of polarization j (only polarization 1 is input, so $E_{f2} = 0$), and

$$E_{rj} = r_j E_{fj} + it_j E_{sj}, \tag{1}$$

is the throughput amplitude of polarization j. E_{sj} is the intracavity mode amplitude just before output coupling, and the input/output coupling coefficient is it_j, with $r_j^2 = 1 - t_j^2 = 1 - T_j$. The input and output coupling coefficients are taken to be equal, as described in Ref. 1.

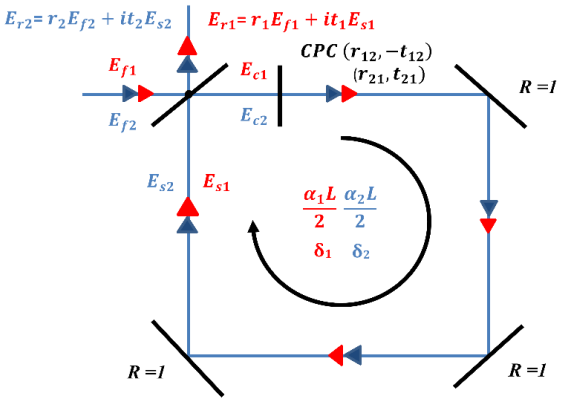

Fig. 1. Ring cavity model representing tapered-fiber coupling to a microresonator with intracavity cross-polarization coupling..

In Fig. 1, δ_j and $\alpha_j L$ are the round-trip phase (modulo 2π) and intrinsic loss for mode j; L is the resonator circumference. Cross-polarization coupling is represented in Fig. 1 as an effective intracavity wave plate and expressed by the coefficients t_{12} and t_{21}, where $t_{12}^2 = 1 - r_{12}^2$ and $t_{21}^2 = 1 - r_{21}^2$ are the polarization rotation probabilities per round trip, called T_s and T_p in Ref. 14.

The intracavity mode amplitudes E_{sj} satisfy the following time evolution equations:

$$\begin{aligned} \frac{d}{dt}E_{s1} &= -\gamma_1 E_{s1} - \frac{t_{12}}{\tau_{rt1}}E_{s2} + \frac{it_1}{\tau_{rt1}}E_{f1} \\ \frac{d}{dt}E_{s2} &= -\gamma_2 E_{s2} + \frac{t_{21}}{\tau_{rt2}}E_{s1} + \frac{it_1 t_{21}}{\tau_{rt2}}E_{f1} \end{aligned}, \tag{2}$$

With these and Eq. (1), the time evolution of the throughput amplitudes can be found. In Eqs. (2), $\tau_{rtj} = n_j L/c$ is the round-trip time for mode j, where n_j is the effective refractive index of the mode, and

$$\gamma_j = \frac{T_j + \alpha_j L}{2\tau_{rt_j}} - i\frac{\delta_j}{\tau_{rt_j}} = \kappa_j(1 + i\theta_j), \tag{3}$$

with κ_j being the amplitude decay rate, or half the inverse of the photon lifetime in mode j, and θ_j being the offset of the resonant frequency of mode j from the input frequency in units of half the mode linewidth.

All parameters appearing in Eqs. (1)-(3) except for t_{21} and t_{12} are related to experimentally measurable quantities, such as quality factors Q_j, resonant dip depths M_j, coupling regime, and detuning Δ of mode 2 from coresonance with mode 1, as

described in Ref. 1. The model is solved in steady state, and $\left|\frac{E_{r1}}{E_{f1}}\right|^2$ and $\left|\frac{E_{r2}}{E_{f1}}\right|^2$, as functions of δ (proportional to detuning of input frequency from mode 1 resonance), are plotted and fit to the experimental throughput spectra of modes 1 and 2 respectively, by choosing values of the two fitting parameters T_c and b. A good fit thus determines T_c and b from experimental data, demonstrating (if $b \neq 1$) the nonreciprocity of CPC.

To illustrate what this model predicts, Fig. 2 shows a simulated case of ATS (CMIT becomes ATS when the coupling is strong enough that $T_c > \kappa_1\kappa_2\tau_{rt1}\tau_{rt2}$), showing the throughput spectra of the two modes. The assumed parameter values are all experimentally realistic. Frequency-split dips are observed in the mode 1 throughput and split peaks in the mode 2 throughput.

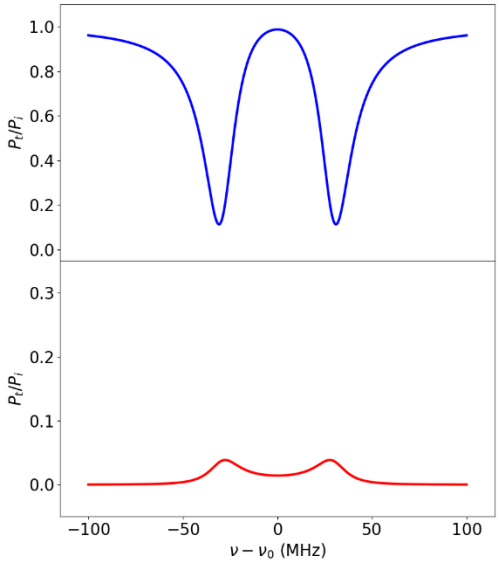

Fig. 2. ATS simulated in an HBR of 90 μm radius. Parameter values: $Q_1 = 5\times10^6$, $Q_2 = 2\times10^8$; $M_1 = 0.9$ (undercoupled), $M_2 = 0.1$ (undercoupled); $\Delta = 0$ MHz. Assumed coupling strength: $T_c = 1.79\times10^{-7}$ and $b = 4$.

The significance of the CPC strength T_c and the nonreciprocity ratio b can be seen in Fig. 3. In the left and right panels, the value of T_c is the same and the mode 1 throughput spectra are identical. Left and right have different values of b, and the height of the mode 2 peak is proportional to b. In Fig. 3, the value of T_c is small enough that mode 1 shows a CMIT feature and mode 2 a single peak. All simulations and experimental results shown here involve HBRs of two slightly different sizes: an HBR with an outer radius of 90 μm will have an inner radius of 76 μm, and an HBR with an outer radius of 98 μm will have an inner radius of 85 μm.

As described in detail in Ref. 14, CPC resulting from the optical spin-orbit interaction will be asymmetric or nonreciprocal, in that the coupling from TE to TM will have a different amplitude from the coupling from TM to TE ($t_{21} \neq t_{12}$). These amplitudes can be calculated by using coupled-mode theory to account for the effects of spatial overlap and phase mismatch between the two orthogonally polarized WGMs.

The radial part of the mode function of a WGM is given in terms of Bessel functions in the three regions of the HBR, interior, silica wall, and exterior. For a small range around a given wavelength (1550 nm), multiple solutions will exist for various combinations of the mode numbers m (number of wavelengths in the circumference) and p (number of radial intensity lobes). One solution is found for the TM mode and one for the TE mode, and their radial overlap is calculated. Then for each mode, a value of the mode number q (number of zeros in an axial intensity plot) is assumed, and the overlap of the two axial profiles, each having the form of a Hermite polynomial of order q times a Gaussian, is calculated. Then the method of Ref. 14 is used to find the CPC strengths. There are two possibilities: the input mode 1 can be TM or TE, making mode 2 the other polarization. The value of T_c is calculated, and the values of b for the two possibilities are then found. An example is shown in Fig. 4.

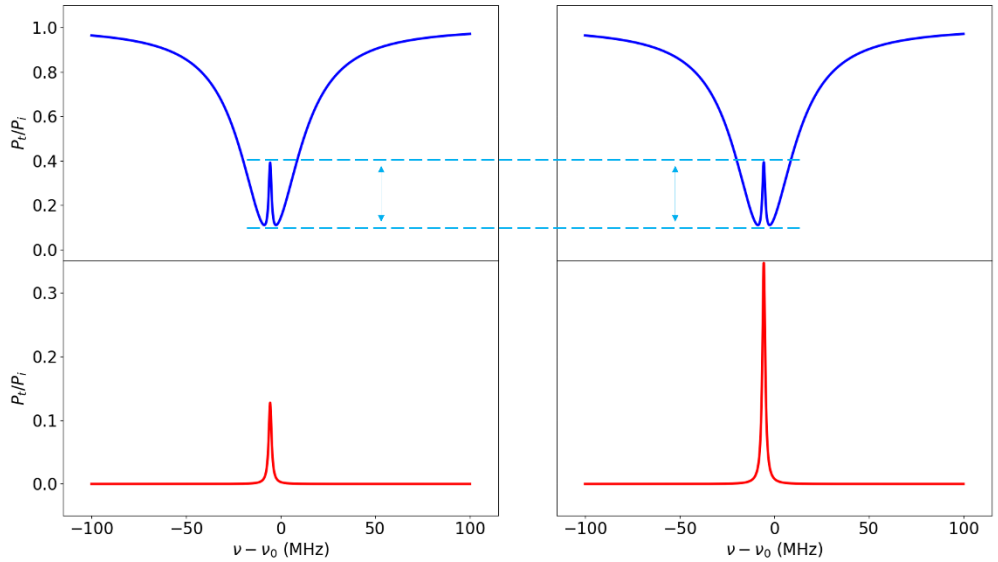

Fig. 3. CMIT simulated in an HBR of 98 μm radius. Parameter values: $Q_1 = 5\times10^6$, $Q_2 = 2\times10^8$; $M_1 = 0.9$ (undercoupled), $M_2 = 0.5$ (undercoupled); $\Delta = 0$ MHz. Assumed coupling strength: $T_c = 2.65\times10^{-8}$. Left: $b = 2.56$; right: $b = 6.97$.

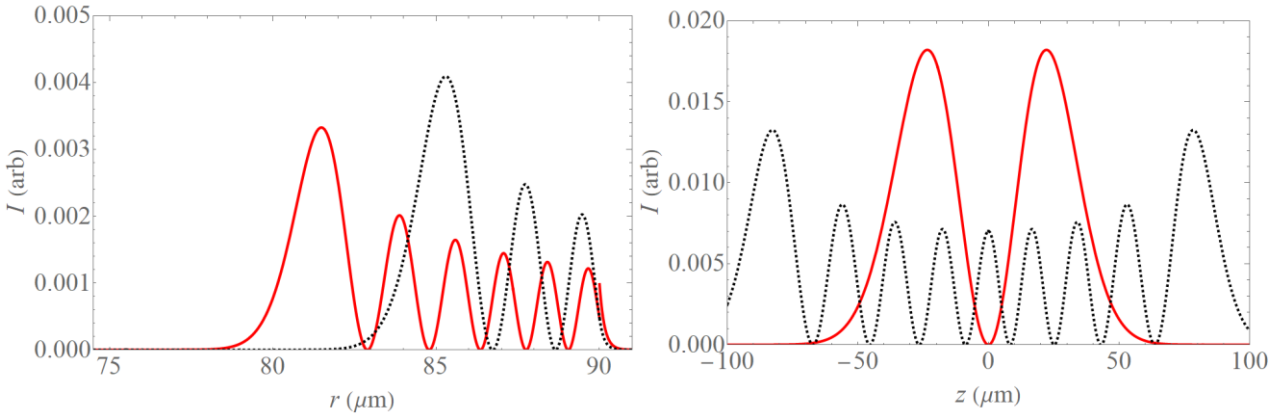

Fig. 4. Radial (left) and axial (right) intensity profiles for a 90-μm-radius HBR. TM (solid red): $m = 471$, $p = 6$, $q = 1$. TE (dashed black): $m = 491$, $p = 3$, $q = 8$. $T_c = 3.07\times10^{-8}$. If TE input, $b = 2.28$; if TM input, $b = 0.439$.

3. EXPERIMENTAL RESULTS

3.1. Experimental setup

The experimental setup used is shown in Fig. 5. The tunable diode laser is scanned in frequency and its free-space beam passes through an acousto-optic modulator. Wave plates and a compression-based polarization controller are used to control the input polarization. The coupling fiber is made adiabatically bi-tapered and brought into contact with the HBR in its equatorial plane using a 3D translation stage (not shown). The HBR is mounted on a piezo-controlled holder for strain tuning. The length of fiber after the HBR is kept short and straight to preserve the polarization.

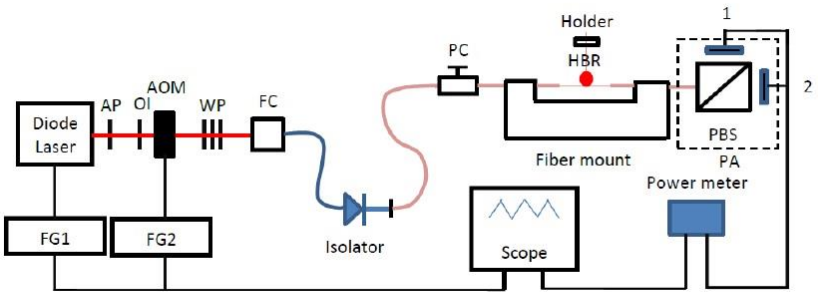

Fig. 5. Experimental setup.

In all cases, the resonator is kept inside an acrylic box to minimize temperature fluctuations and other effects of air movement. The output signal is sent to a polarization analyzer (PA), which includes a polarizing beam splitter (PBS) plus two matched fast detectors and can be rotated about the fiber axis so that either detector can detect either polarization. For data analysis, the detector signals are separately input to the oscilloscope, without using the power meter shown in Fig. 5.

3.2. Typical results

Light of one polarization is input, and the HBR is strain-tuned to TE-TM coresonance, resulting in the throughput spectrum of the input polarization showing an ATS feature, while the output of the other polarization shows a peak resulting from intracavity CPC. Individual mode parameters, as described below Eq. (3), are measured by tuning away from coresonance and using input of the two polarizations sequentially. Using those parameters, the model is fitted, using the method described in Ref. 1, to the experimental spectral traces by choosing values of the two free parameters T_c and b. Figures 6 and 7 show two cases. The outer radius of the HBR is given in each case; also, based on the method of HBR fabrication as described in Ref. 15 but without using the hydrofluoric acid etching solution to thin the silica wall, the inner radius is estimated to be 76 μm when the outer radius is 90 µm, and 85 μm when the outer radius is 98 μm.

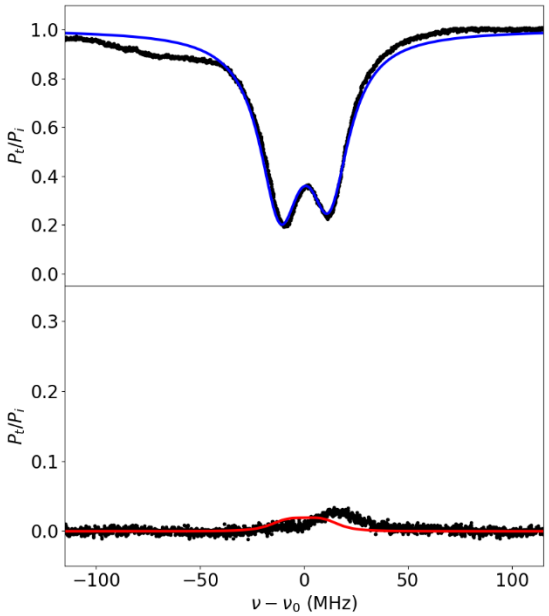

Fig. 6. ATS with 98-μm-radius HBR and TE input. Experimental (black traces) and numerical fitting (blue and red lines) throughput spectra. Parameter values: $Q_1 = 6.95\times10^6$, $Q_2 = 9.93\times10^6$; $M_1 = 0.965$ (undercoupled), $M_2 = 0.285$ (undercoupled); $\Delta = 1.69$ MHz. From the fit it is found that $T_c = 4.71\times10^{-8}$ and $b = 0.62$.

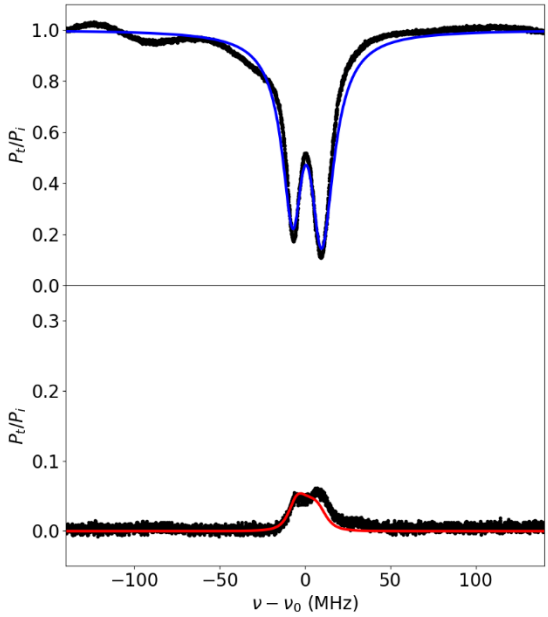

Fig. 7. ATS with 98-μm-radius HBR and TE input. Experimental (black traces) and numerical fitting (blue and red lines) throughput spectra. Parameter values: $Q_1 = 8.80\times10^6$, $Q_2 = 2.26\times10^7$; $M_1 = 0.95$ (undercoupled), $M_2 = 0.13$ (undercoupled); $\Delta = -2.77$ MHz. From the fit it is found that $T_c = 2.26\times10^{-8}$ and $b = 4.12$.

In Figs. 6 and 7, the experimental peak on the orthogonal-polarization (mode 2) output has a shape that is slightly different from the prediction of the model. This is most likely due to interaction with another mode of the same polarization, slightly overlapping in frequency with the mode that couples to the input-polarization mode via CPC.

4. DISCUSSION

Our earlier theoretical work showed that the cross-polarization coupling that is responsible for CMIT, CMIA, and ATS in a whispering-gallery microresonator is nonreciprocal. Our previous experimental work allowed us to determine the effective CPC strength T_c that determines the throughput spectrum of the input polarization. Now, by observing the output of the polarization orthogonal to the input, we can demonstrate CPC nonreciprocity and find the two unequal CPC amplitudes. Further, the theory can be used to find possible candidates for the mode numbers of the two WGMs involved.

The fitting method assumes that only two modes are interacting, and it was seen that a third mode near coresonance with the main two can affect the shape of the peak observed in the orthogonal output. The experimental results of Figs. 6 and 7, along with the theoretical calculations and simulations, are for an empty HBR, so that the internal and external regions both have a refractive index of 1. However, other experiments have been done on water-filled and methanol-filled HBRs. It was hoped that a mode of high enough radial order could be excited so that the input mode (mode 1) would have a significantly lower Q than mode 2, owing to absorption losses in the interior. This would have produced a greater possibility to see CMIT, not just ATS. This is still under investigation, and it is a relatively simple matter to modify the theory correspondingly. Based on calculations like those of Fig. 4, the HBR wall will have to be thinned by etching or by making the bulge significantly larger to have WGMs with internal fractions.

With the understanding gained here about the orthogonally polarized output 2 under conditions of CPC, its implementation is enabled to a greater degree. Preliminary model results have shown that in some cases the pulse delay of output 2 can be significantly larger than the delay of the output 1 pulse of input polarization. In addition, its amplitude can be greater than that of the output 1 pulse, under certain conditions, if b is large enough. Thus, the non-reciprocity of CPC can have potentially useful consequences.

ACKNOWLEDGMENT

We would like to thank Sreekul Raj Rajagopal for assistance with the experiments.

REFERENCES

[1] Bui, K. V., and Rosenberger, A. T., "Coupled-mode-induced transparency and attenuation resulting from cross-polarization coupling," Phys. Rev. A 101, 033836 (2020).

[2] Totsuka, K., Kobayashi, N., and Tomita, M., "Slow light in coupled-resonator induced transparency," Phys. Rev. Lett. 98, 213904 (2007).

[3] Zhou, X., Zhang, L., Pang, W., Zhang, H., Yang, Q., and Zhang, D., "Phase characteristics of an electromagnetically induced transparency analogue in coupled resonant systems," New J. Phys. 15, 103033 (2013).

[4] Foreman, M. R., Swaim, J. D., and Vollmer, F., "Whispering gallery mode sensors," Adv. Opt. Photon. 7, 168-240 (2015).

[5] Yoshiki, W., Honda, Y., Tetsumoto, T., Furusawa, K., Sekine, N., and Tanabe, T., "All-optical tunable buffering with coupled ultra-high *Q* whispering gallery mode microcavities," Sci. Rep. 7, 10688 (2017).

[6] Smith, D. D., Chang, H., Myneni, K., and Rosenberger, A. T., "Fast-light enhancement of an optical cavity by polarization mode coupling," Phys. Rev. A 89, 053804 (2014).

[7] Konishi, H., Fujiwara, H., Takeuchi, S., and Sasaki, K., "Polarization-discriminated spectra of a fiber-microsphere system," Appl. Phys. Lett. 89, 121107 (2006).

[8] Ramelow, S., Farsi, A., Clemmen, S., Levy, J. S., Johnson, A. R., Okawachi, Y., Lamont, M. R. E., Lipson, M., and Gaeta, A. L., "Strong polarization mode coupling in microresonators," Opt. Lett. 39, 5134-5137 (2014).

[9] Liu, Y. C., Li, B.-B., and Xiao, Y.-F., "Electromagnetically induced transparency in optical microcavities," Nanophotonics 6, 789-811 (2017).

[10] Nasir, M. N. M., Gorajoobi, S. B., Murugan, G. S., and Zervas, M. N., "Polarization effects in optical microresonators," J. Opt. Soc. Am. B 36, 705-716 (2019).

[11] Kreismann, J., and Hentschel, M., "Spin-orbit interaction of light in three-dimensional microcavities," Phys. Rev. A 102, 043524 (2020).

[12] Wang, C., Jiang, X., Sweeney, W. R., Hsu, C. W., Liu, Y., Zhao, G., Peng, B., Zhang, M., Jiang, L., Stone, A. D., and Yang, L., "Induced transparency by interference or polarization," Proc. Natl. Acad. Sci. USA 118, e2012982118 (2021).

[13] Rosenberger, A. T. and Bui, K. V., "Mode-superposition-induced transparency," Proc. SPIE 12016, to be published.

[14] Rosenberger, A. T., Dale, E. B., Bui, K. V., Gonzales, E. K., Ganta, D., Ke, L., and Rajagopal, S. R., "Cross-polarization coupling of whispering-gallery modes due to the spin-orbit interaction of light," Opt. Lett., 44, 4163-4166 (2019).

[15] Stoian, R.-I., Bui, K. V., and Rosenberger, A. T., "Silica hollow bottle resonators for use as whispering gallery mode based chemical sensors," J. Opt. 17, 125011 (2015).

[16] Ke, L., Rajagopal, S. R., and Rosenberger, A. T., "Numerical and experimental study of the dynamics of cross-polarization coupling in a whispering-gallery microresonator," Proc. SPIE 10904, 109041T (2019).

[17] Ke, L., Rajagopal, S. R., and Rosenberger, A. T., "Dynamical determination of the strength of cross polarization coupling in a single whispering-gallery microresonator," Phys. Rev. A. 104, 053534 (2021).